Journal of Materials Chemistry A

Hydronium Ion Diffusion in Model Proton Exchange Membranes at Low Hydration: Insights from Ab Initio Molecular Dynamics

Journal:	*Journal of Materials Chemistry A*
Manuscript ID	TA-ART-10-2020-010565.R1
Article Type:	Paper
Date Submitted by the Author:	24-Dec-2020
Complete List of Authors:	Zelovich, Tamar; New York University, Chemistry Winey, Karen; University of Pennsylvania, Materials Science & Engineering Tuckerman, Mark; New York University, Department of Chemistry and Courant Institute of Mathematical Sciences

Hydronium Ion Diffusion in Model Proton Exchange Membranes at Low Hydration: Insights from Ab Initio Molecular Dynamics

Tamar Zelovich$^{(1)}$, Karen I. Winey$^{(2)}$, and Mark E. Tuckerman$^{(1),(3),(4)*}$

1) Department of Chemistry, New York University (NYU), New York, New York 10003, United States

2) Department of Materials Science and Engineering, University of Pennsylvania, Philadelphia, Pennsylvania 19104, United States

3) Courant Institute of Mathematical Sciences, New York University (NYU), New York, New York, 10012, United States

4) NYU-ECNU Center for Computational Chemistry at NYU Shanghai, 3663 Zhongshan Rd. North, Shanghai, 200062, China

Email: mark.tuckerman@nyu.edu

Abstract

Fuel-cell deployable proton exchange membranes (PEMs) are considered to be a promising technology for clean and efficient power generation. However, a fundamental atomistic understanding of the hydronium diffusion process in the PEM environment is an ongoing challenge. In this work, we employ fully atomistic *ab initio* molecular dynamics to simulate diffusion mechanisms of the hydronium ion in a model PEM. To mimic a precise polymer with a layered morphology, recently introduced by Trigg, *et al*. [*Nature Materials* **17**, 725 (2018)], a nano-confined environment was created composed of graphane bilayers to which sulfonate end groups (SO_3^-) are attached, and the space between the bilayers was subsequently filled with water and hydronium ions up to λ values of 3 and 4, where λ denotes the water-to-anion ratio. We find that for the low λ value, the water distribution is not homogeneous, which results in an incomplete second solvation shell for H_3O^+, fewer water molecules in the vicinity of SO_3^-, and a higher probability of obtaining a coordination number of ~1 for the nearest oxygen neighbor to SO_3^-. These conditions increases the probability that H_3O^+ will react with SO_3^- according to this reaction: $SO_3^- + H_3O^+ \leftrightarrow SO_3H + H_2O$, which was found to be an essential part of the hydronium diffusion mechanism. This suggest there are optimal hydration conditions that allow the sulfonate end groups to take an active part in the hydronium diffusion mechanism, resulting in high hydronium conductivity. We expect the results of this study may help guide

synthesis and experimental characterization used to design new PEM materials with high hydronium conductivity.

Introduction

Fuel cell deployable proton exchange membranes (PEMs) have been studied extensively over the last few decades due to their promise in technologies for clean and efficient power generation.[1-12] In recent years, nano-confined environments have been exploited in the study of cost-effective and reliable polymer architectures for electrochemical devices.[13-21] Understanding the behavior of waters and ions in these confined environments is essential to gain insight into the ions' diffusion mechanisms within these devices.

The three structural facets that must be considered in the design of new PEMs under nano-confinement are: (a) the polymer backbone and associated mesoscale morphology, (b) an anionic group, and (c) a tether that connects the anionic group to the polymer. The sulfonate anionic functional end group (SO_3^-) is one of the most widely used groups in PEM fuel cell devices.[22-31]The protonation state of SO_3^- and its dependence on water content and temperature in the system have been studied extensively by the use of techniques such as NMR [32-34], vibrational spectroscopy [35,36], Raman spectroscopy [37] and X-ray scattering.[38,39] Specifically, properties such as PEM morphology and the local structure of the sulfonate-terminated side chains have received increased attention both experimentally [40-44] and theoretically.[40,42,45-48] Several studies suggest that the sulfonate end group appears in a deprotonated state (i.e., SO_3^-) in hydrated systems, or in a protonated state (i.e., SO_3^-H) at low-hydration conditions. In some cases, it was argued that the hydronium diffusion mechanism is mainly vehicular under low hydration conditions, whereas there is a significant contribution from the structural diffusion at high hydration conditions. [28,42,49-51]

Despite the abundance of studies in the field of PEMs, ongoing discussion continues about the role of the protonation state of SO_3^- in the underlying atomistic picture governing the hydronium ion diffusion process. At a more fundamental level, elementary steps governing proton transport phenomena in hydrogen-bonded media continue to be of considerable interest to the physical chemistry community. Understanding and controlling the proton transport mechanism on the atomistic level is essential in order to develop PEMs with high hydronium conductivity.

The computational methods most frequently used to study the SO_3^- end groups in PEMs include mesoscopic simulations [40,42,45,46,48,51-55], classical molecular dynamics (MD) simulations [4,49,50,56-59], and density functional theory (DFT) calculations.[5,22,52,60] On a more fundamental level, although some *ab initio* molecular dynamics (AIMD) simulations [28,61-64] have been performed over the past decade, the high computational burden of such an approach has limited its use in this area. Nevertheless, the use of AIMD, in which the interatomic forces are computed "on the fly" from density functional theory (DFT) based electronic structure calculations as the simulation proceeds, is critical when studying aqueous hydronium and hydroxide diffusion. As was shown in Ref. 65, AIMD predicted a fourth weak hydrogen bond to the hydronium ion in the proton transfer (PT) process. This result was later used to parameterize new multistate empirical valence bond models.[66] Such empirical models cannot be easily transferred to different chemical environments, as we investigate here. The trade-offs in the use of AIMD over a reactive force field are the usual limitations in accessible length and time scales. These limitations require careful selection of the systems to be studied.

Recently, we used fully atomistic AIMD simulations to study hydroxide diffusion in model anion exchange membranes (AEMs) using nano-confined environments consisting of graphane bilayers (GBs) as mimics of the actual polymer architectures.[67-70] We find that factors that control hydroxide diffusion in these systems, including local coordination patterns and pre-solvation mechanisms, were shown to differ from those in bulk solution [71-81] in a way that is strongly influenced by the shape and size of the confining volume, the hydration level, and the cation spacing.

In this study, we apply a similar protocol to explore hydronium diffusion in two architecturally distinct PEMs, employing nano-confined volumes inspired from our previous studies. [67-70] The choice of GBs to mimic a particular polymer architecture with a layered morphology in the study of PEMs was inspired by a recent study of Trigg, *et al.* 7, in which it was shown that well-ordered and hydrated membranes with highly crystalline morphology have the potential to achieve high proton conductivity. We find that the protonation state of SO_3^- changes during the course of the simulation, as under specific conditions, the following reaction occurs: $SO_3^- + H_3O^+ \leftrightarrow SO_3H + H_2O$. This study aims to uncover both the conditions required for this reaction to occur and the role of this reaction in the hydronium diffusion mechanism. In addition, we present a comparison of our findings to previously studied hydroxide diffusion mechanisms in analogous AEM environments. We believe that identifying the differences in the diffusion mechanisms of ions in PEMs and AEMs will help reveal key principles for new stable membrane materials with high ion conductivity for use in fuel cell device applications.

2. Description of Systems

In this study, we explored two different GB systems representing two model PEM environments, in which the nanoconfined structure in these systems mimics the layered arrangement recently reported in Ref. 7. Each system contains two identical graphane layers aligned in the *xy*-plane, two SO_3^- anions attached to the GBs using a $(CH_2)_2$ linker, two hydronium ions (whose oxygen cores are denoted O^*_1 and O^*_2), and a variable number of water molecules. The two anions are attached by the linkers to fixed points in the GBs but are otherwise free to move in the aqueous solution. The two attachment points define the polymer electrolyte anion spacing in the *x* and *y* directions (see Figure 1). Based on Refs 7 and 82, the tunable parameters for the two systems are: (i) the hydration level, λ, chosen to be 3 or 4, (ii) the distance between the two carbon sheets, Δz, fixed at 7.3 Å for all systems (see Refs 67 and 68 for rationale), and (iii) the polymer electrolyte cation spacing in the *x* and *y* directions, as measured between two sulfur atoms (Δx and Δy), in which Δx and Δy are fixed at 10 Å and 6.6 Å, respectively, for the two systems. For clarity, we refer to the two systems as **λ3** and **λ4,** in which the numbers represent the respective hydration levels.

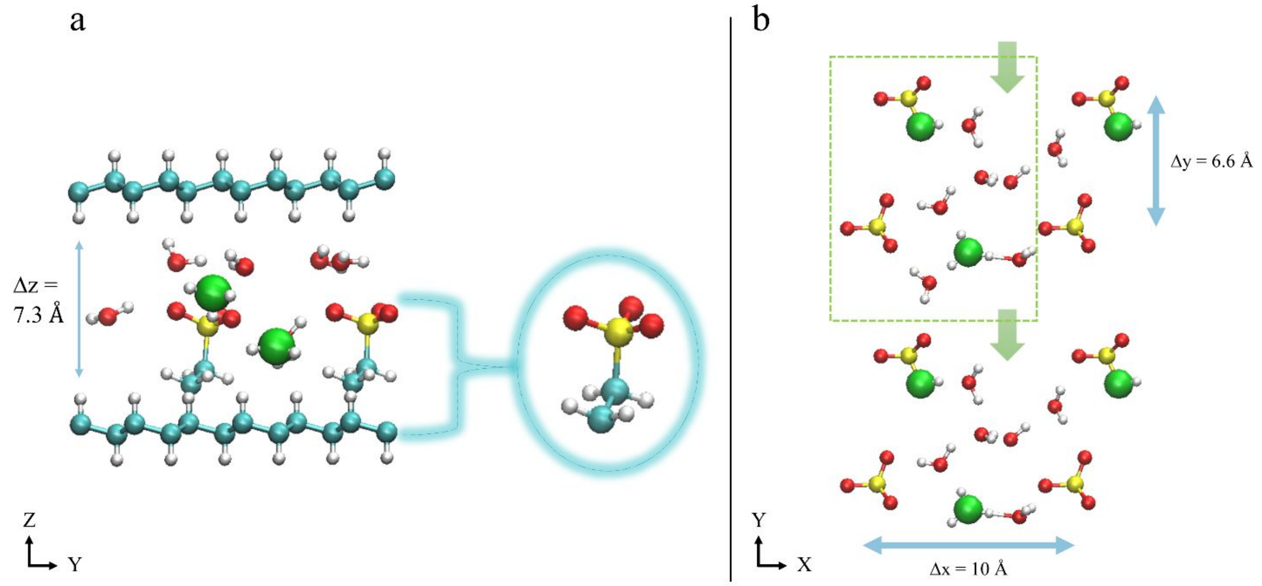

Figure 1: (a) A side perspective of the atomistic graphane bilayer (GB) models, each consisting of two graphane sheets with two SO_3^- anions, two hydronium ions, and enough water molecules to reach the required value of λ. The two GB systems are fully hydrogenated except for the two attachment points of the anions. The red, white, turquoise, and yellow spheres represent O, H, C, and S atoms, respectively. The green spheres show the position of hydronium ion oxygens. The turquoise arrow demonstrates the distance between the two carbon sheets. (b) The view of the PEM model system along the *z*-direction (with the upper and lower graphane sheets removed for clarity). The green rectangle shows the primitive simulation cell of the system. The green arrows demonstrate the hydronium ion diffusion path. The turquoise arrows demonstrate the polymer electrolyte cation spacing in the *x* and *y* directions.

3. Computational Method

Once the desired starting structures were generated, AIMD simulations [83] were performed using the CPMD code.[84,85] Each system was equilibrated at room temperature using a massive Nosé-Hoover chain thermostat [86], followed by 15-20 ps of canonical (NVT) dynamics, also using a massive Nosé-Hoover chain thermostat, and finally ~80 ps of microcanonical (NVE) dynamics. To account for dispersion forces, we employed the Dispersion-Corrected Atomic Core Pseudopotentials (DCACP) scheme[87,88] within the Kohn-Sham formulation of Density Functional Theory using the B-LYP exchange-correlation functional.[89,90] The performance B-LYP+DCACP has previously been shown to give satisfactory results for water-acene interactions[91], for liquid water [92], and for hydronium diffusion in bulk water.[65,71-73] A detailed description of the computational method can be found in our previous work. [67-70]

4. Results

4.1 Solvation Structures

The primary aim of this work is gain insight into how changing the water content affects hydronium diffusion in the model systems employed. To this end, we begin by exploring the solvation structures of the water molecules, the hydronium ions, and the sulfonic acid end groups.

4.1.1 Water Structure

Figure 2 shows the spatial populations of oxygen atoms in the *xy*-plane generated from the trajectory. This allows us to glean the preferred locations of water molecules and provides a clear picture for the water density profile in the *xy*-plane. The results show that the water distribution in the cell of system **λ3** is not uniform. However, for system **λ4**, which has one extra water molecule per cation than does **λ3**, the water distribution was found to be uniform. Inspection of the configurations from the AIMD trajectories support these findings (see Figure 2). Specifically, for system **λ3,** we find that void areas are formed in parts of the simulation cell. At this low level of hydration, all waters in the system can be regarded as interfacial, that is, in contact with some part of the “membrane”, and inhomogeneously distributed throughout the system. Furthermore, we find that the non-uniform/uniform water distribution for systems **λ3** and **λ4**, respectively, persists throughout the simulation.

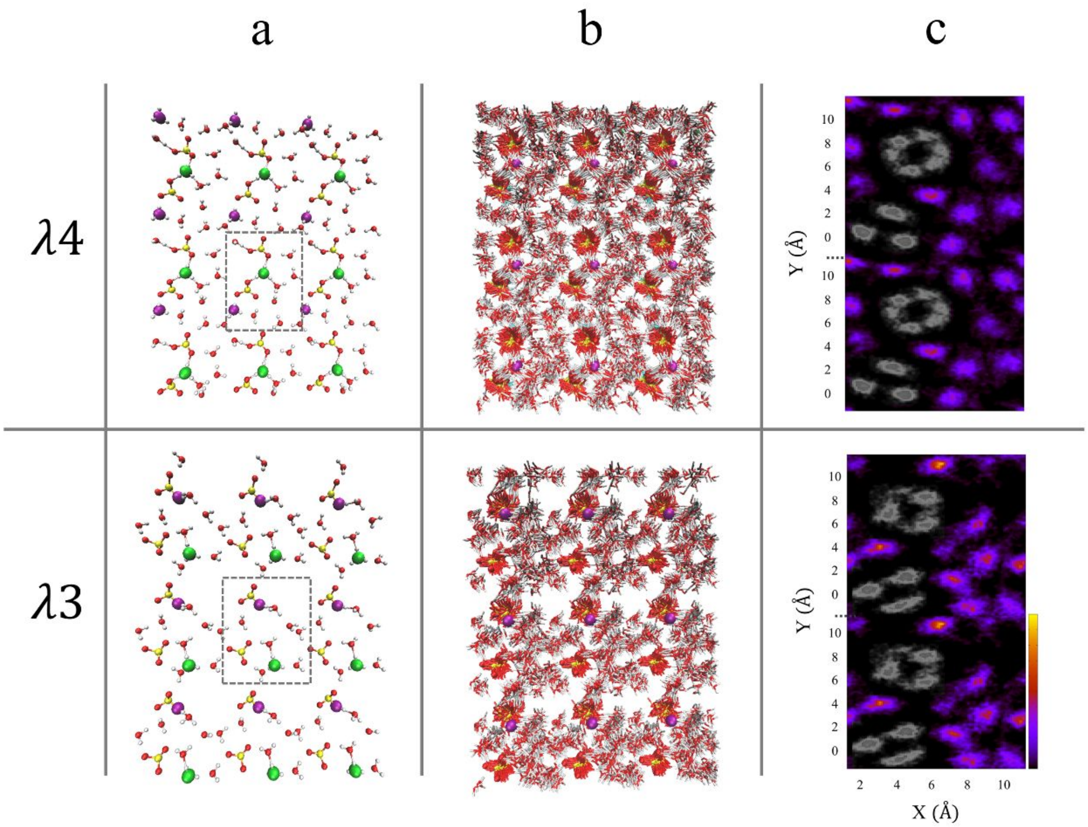

Figure 2: The view of systems **λ3** and **λ4** along the *z*-direction (with the upper and lower graphane sheets removed for clarity). (a) Representative snapshots and (b) Superposition of configurations sampled every 0.96 ps from the NVE trajectory. The red, white, turquoise, and yellow spheres represent O, H, C, and S atoms, respectively. The green and purple spheres represent the positions of hydronium ion oxygens. The grey rectangles show the primitive simulation cell of the system. (c) Water density profile presented by spatial population of the oxygens in the *xy*-plane. The grey areas represent the locations of the anions throughout the simulations, and the bar color depicts the probability density of the water oxygens locations in the *xy*-plane, normalized according to the number of time steps obtained in the simulation, independent of the *z*-coordinates of the oxygens. The black dotted line shows the primitive simulation cell of the system on the *y*-direction.

Unlike in bulk solution, in which the water oxygen has, on average, a fourfold-tetrahedral coordination pattern, the low hydration values in the two systems result in a first solvation shell of approximately three for the water oxygens, in which two are water oxygens and one is an anion oxygen, as seen in the OO radial distribution function (RDF) presented in the Supporting Information (SI). The differences in the water distribution between the two systems are pronounced in the second solvation shell of the water oxygens, for example, the integrated coordination numbers (CNs) of the second solvation shell are approximately 4 and 5 for systems **λ3** and **λ4**, respectively.

These differences in water distribution at low hydration were previously seen in our recent work on low hydrated AEMs.[68] Furthermore, it was shown that the hydroxide ion diffusion is vehicular for non-uniform water distributions, and structural for uniform water distributions. Similar to the AEMs, we find that for PEMs, the water distribution affects the hydronium ion diffusion. However, as will be discussed in the next sections, the hydronium diffusion mechanism in PEMs is fundamentally different from the hydroxide diffusion mechanism found for AEMs.

4.1.2 H_3O^+ Solvation Structure

We turn next to an exploration of the hydronium ion solvation structure. For this purpose, we plot, in Figure 3, the O*O RDF and CNs (O* represents the hydronium oxygens and O represents SO_3^- and water oxygens). As shown, the first solvation shell peak is located at 2.6 Å for both systems, and the CN values of the first solvation shell of the two systems is 3.1, as was previously found for bulk solution.[71] Furthermore, we find that the oxygens taking part in the hydronium solvation complex are both water and SO_3^- oxygens (see inset of Figure 3 for examples). To support these results, we calculated the population probabilities for the H_3O^+ solvation complexes; these populations indicate that the most likely complex is 3A+0D with 90% and 86% for systems **λ3** and **λ4**, respectively (see hydrogen bond (HB) criteria in SI).

While the first solvation shell of the hydronium ion is approximately identical in the two systems, we find that the difference between the hydronium solvation structures is pronounced in the second solvation shell, with CN values of 7.5 and 8.5 for systems **λ3** and **λ4**, respectively (including the SO_3^- oxygens). Excluding the first solvation shell oxygens and the SO_3^- oxygens, the number of water oxygens in the second solvation shell of the hydronium ions are 1.5 and 2.5 for systems **λ3** and **λ4**, respectively. This suggests the hydronium ions in system **λ3** are missing a complete second solvation shell as a result of the non-uniform water distribution that develops in this system (to support these results, the O*O_w RDF and CNs are presented in the SI).

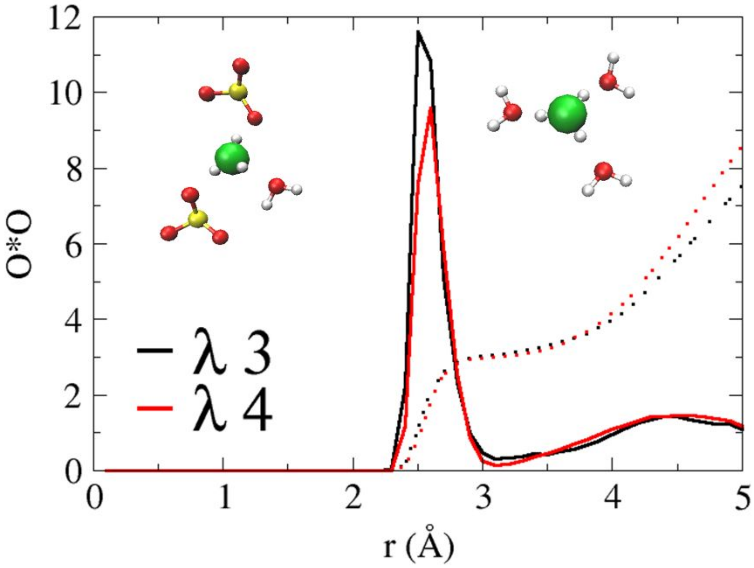

Figure 3: Radial distribution functions for systems **λ3** and **λ4** (black and red curves, respectively) of O*O. The colored dotted lines represent the obtained coordination numbers. Inset: two examples of hydronium ions in a threefold solvation complex.

4.1.3 SO_3^- Solvation Structure

To explore the solvation structure of SO_3^- oxygens, we plot the OsO RDF and CNs for the two systems in Figure 4 (Os represents SO_3^- oxygens, and O represents all other oxygens in the system). As shown, the first and second peaks, which represent the first and second solvation shells, are located at approximately the same value of *r* for the two systems. A comparison of the CN values (Figure 4b) shows elevated numbers for system **λ4** for both the first and second solvation shells with values of 1.8 and 4.1, respectively, compared to values of 1.5 and 3.3 for **λ3** . This result, which is a direct outcome of the higher hydration values in system **λ4**, shows that the second solvation shell of the SO_3^- oxygens in system **λ4** contains one extra water oxygen compared to system **λ3**.

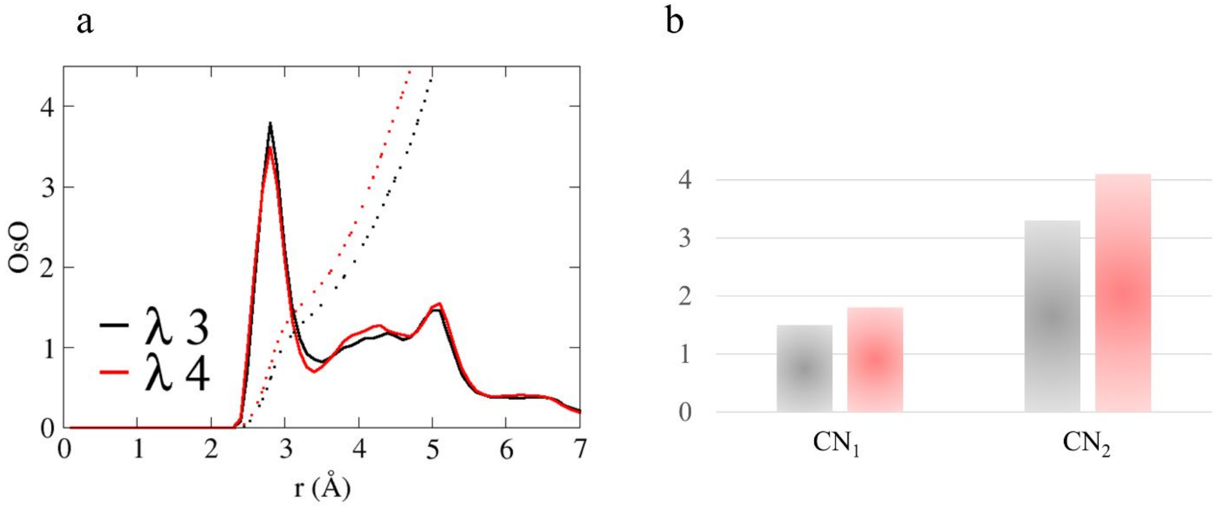

Figure 4: (a) Radial distribution functions for systems $\boldsymbol{\lambda 3}$ and $\boldsymbol{\lambda 4}$ (black and red curves, respectively) of OsO (Os represents SO_3^- oxygens and O represents all other oxygens in the system). The colored dotted lines represent the obtained coordination numbers. (b) Specified coordination numbers for the first (CN_1) and second (CN_2) solvation shells, for systems $\boldsymbol{\lambda 3}$ and $\boldsymbol{\lambda 4}$ (black and red bars, respectively).

4.2 H_3O^+ Diffusion Mechanism

In order to shed light on the transport process of hydronium ions in this confined environment, we calculate water and hydronium diffusion constants along each of the axes separately (see Table 1). These components can be interpreted as the diagonal elements of the diffusion tensor, an important quantity in the calculation of ionic conductivities.[67-70] In the SI, we present a simple time trace of the coordinates of the hydronium oxygens along the trajectory.

Table 1: Diffusion constants obtained from the slope of the Mean Square Displacement as presented in Supplementary Information (all in units of Å^2/ps).

	$\mathbf{D_{H_3O^+}}$				$\mathbf{D_{H_2O}}$			
	D_{ave}	D_X	D_Y	D_Z	D_{ave}	D_X	D_Y	D_Z
System λ3	0.070	0.106	0.095	0.010	0.039	0.083	0.036	0.001
System λ4	0.007	0.003	0.011	0.006	0.009	0.006	0.004	0.017

A comparison of the diffusion constants of the two systems shows that increasing λ from 3 to 4 results in a decrease in the average hydronium ion diffusion constant (0.070 Å^2/ps and 0.007 Å^2/ps for systems **λ3** and **λ4**, respectively). Specifically, system **λ4** is seen to have the lower hydronium diffusion constants along all axes. This agrees with the evolution of the coordinates of the two hydronium ions (SI Figure S2), where both ions are non-diffusive. In system **λ3**, hydronium ion diffusion occurs along the *x*- and *y*-axes, with diffusion tensor components of 0.106 Å^2/ps and 0.095 Å^2/ps along each of these directions, respectively. According to Figure S2 in SI, both ions in system **λ3** become diffusion "activated" (at ~50 ps) after an initial quiescent period. The water molecules were found to be non-diffusive for both systems, suggesting that water diffusion is not required for hydronium ion diffusion (the non-diffusivity of the water molecules accords with the water profile presented in Figure 2).

Further insight into the conditions that enable the diffusion of the two hydronium ions in system **λ3** and suppress their diffusion in system **λ4** can be gleaned by turning to the RDF and CNs for SO* presented in Figure 5a. As shown in the figure, the positions of the first two peaks, which represent the first and second solvation shells, are identical for both systems. The first peak, located at ~1.7 Å, corresponds to SO_3H, in which an H_3O^+ has transferred a proton to an SO_3^-, while the second peak is located at ~3.7 Å. The SO* CN values (specified in Figure 5b) for the first peak are 0.7 and 0.02, and for the second peak are 0.8 and 0.4 for systems **λ3** and **λ4**, respectively (note that, because of the limited system size and small number of S and O* species, the SO* CN does not go to 1 at large *r*, as it would in a larger system with a greater number of these atom types). This suggests that due to the reaction of hydronium with SO_3^- anion to create

SO_3H, the latter neutral species exists for a greater proportion of time in the ***λ*3** system than it does in in ***λ*4**. To verify this, we calculate the percentage of time that the hydronium ions spent as SO_3^- and SO_3H (Figure 5c). As expected, we find that for system ***λ*3**, the hydronium ion appears as SO_3H for 48.78% of the simulation time, while for system ***λ*4**, it appears as SO_3H for only 3.6% of the simulation time. Our results support those of a recent classical molecular dynamics study reported by Sengupta *et al*. 55, who observed that the hydronium ion diffusion decreases with increasing degree of deprotonation. It is important to note that the use of classical molecular dynamics requires fixing the protonation state *a priori*, whereas it can vary naturally in the present AIMD simulations, which means that a direct comparison with the results of Ref. 55 is not possible. It, nevertheless, appears that the protonation state of the sulfonate group plays an important role in the hydronium diffusion process at low hydration.

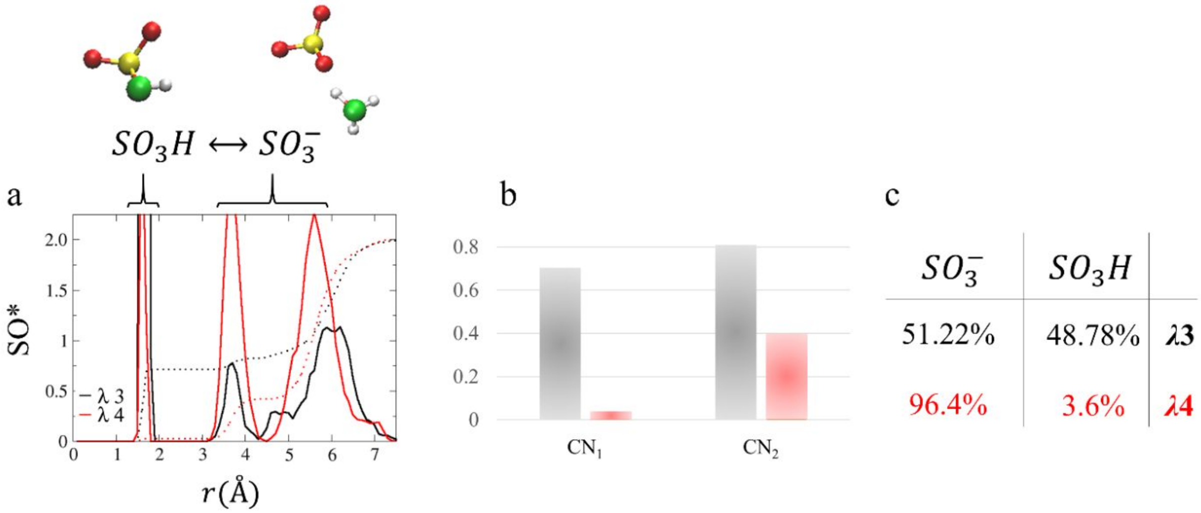

SO_3^-	SO_3H	
51.22%	48.78%	*λ*3
96.4%	3.6%	*λ*4

Figure 5: (a) Radial distribution functions of SO* for systems ***λ*3** and ***λ*4.** The colored dotted lines represent the obtained coordination numbers. (b) Specified coordination numbers for the first and second solvation shells. (c) The time in percentage the hydronium ions spent as SO_3^- and SO_3H (the calculation details are specified in SI). Black and red colors represent systems ***λ*3** and ***λ*4**, respectively.

Beyond the protonation state, however, we conclude, more specifically, that the reaction $SO_3^- + H_3O^+ \leftrightarrow SO_3H + H_2O$, itself, plays an important role in the hydronium ion diffusion mechanism in system ***λ*3**. In order to shed additional light on the conditions that enable this reaction, we shift our focus to O_{next}, where O_{next} is the closest water or hydronium oxygen to the SO_3^- oxygens. In Figure 6a we present the $O_{next}O$ RDF and CNs for the two systems. The first peak is located at 2.7 Å and 2.6 Å for systems **λ3** and **λ4**, respectively (see further discussion in SI). The CN values for the first and second peaks are 1.3 and 5.1 for system **λ3**, and 1.48 and 6.0 for system **λ4**. The CN values found for system **λ3** suggest that before PT occurs between the anion (i.e., SO_3H) and a nascent water molecule, the latter acquires a first solvation shell of one water oxygen and an incomplete second solvation shell.

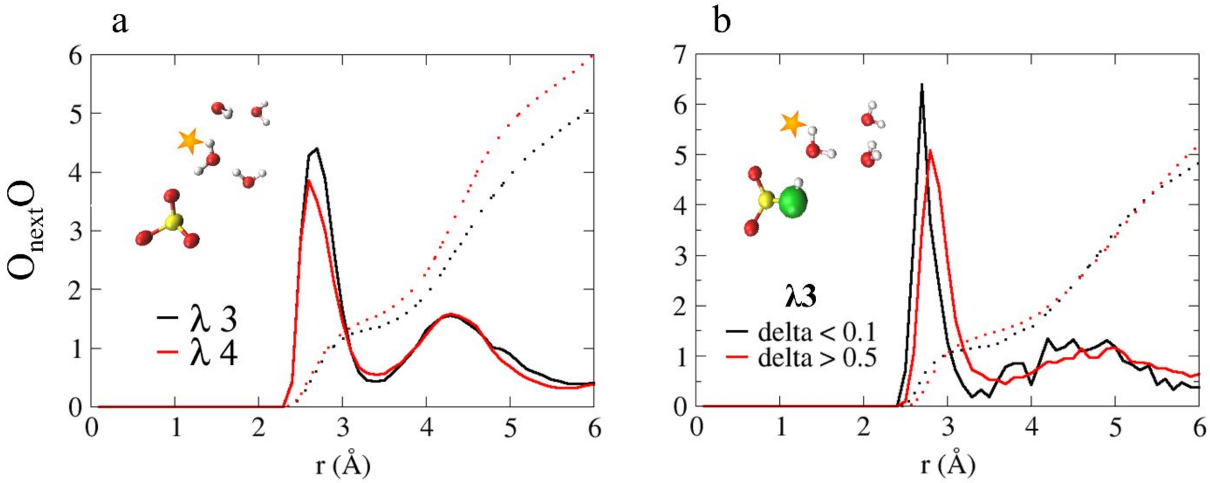

Figure 6: (a) Radial distribution functions of $O_{next}O$ for systems **λ3** and **λ4** (black and red curves respectively). O_{next} represents the first neighbor oxygen to the SO_3^- oxygens and O represents all water and hydronium oxygens. (b) Radial distribution functions of $O_{next}O$ for system **λ3** for $\delta < 0.1$ and $\delta > 0.5$ (black and red curves, respectively). O_{next} represents the first neighbor oxygen to the SO_3H oxygen and O represents all water and hydronium oxygens. The colored dotted lines represent the obtained coordination numbers.

In order to garner additional support for this claim, we investigate system **λ3**, where the reaction is mainly observed, in greater depth. We define a displacement coordinate, $\delta = \left|R_{O_aH} - R_{O_wH}\right|$ where R_{O_aH} and R_{O_bH} are the distances between a shared proton of SO_3H and the nearest water oxygen (i.e., O_{next}). Values of $\delta > 0.5$ are considered to be inactive complexes with respect to PT, while values of $\delta < 0.1$ are considered to be "active" and are associated with PT events.[67,74,75,93,94] In Figure 6b, we present the $O_{next}O$ RDF and CNs for system **λ3** for $\delta < 0.1$ and $\delta > 0.5$, where, in this context, O_{next} represents the first neighbor oxygen to the SO_3H oxygen, and O represents water and hydronium oxygens. We find that for $\delta > 0.5$, the peak is located at 2.8 Å with a CN value of 1.54. However, for $\delta < 0.1$, which is associated with a PT event, the peak is located at 2.7 Å with a CN value of 1.14. This suggests that in order for the reaction to take place, O_{next} is required to have a CN value of ~1.

Combining the results presented in Section 4, we can conclude that the higher reactivity of the hydronium ion seen in system $\boldsymbol{\lambda 3}$ can be explained in terms of the non-uniform water distribution in the system, which results in: (i) a higher probability of obtaining a CN value of ~1 for O_{next}, (ii) an incomplete second solvation shell for the hydronium ions, and (iii) fewer water molecules in the vicinity of the oxygen atoms of the anions (i.e., SO_3^-).

Based on the results above, combined with inspection of configurations from the trajectory, we propose, in Figure 7, an idealized diffusion mechanism for hydronium ions in PEMs under idealized hydration conditions (i.e., system $\boldsymbol{\lambda 3}$). First, three water molecules in the simulation box solvate the hydronium ion, which is located in the center of the cell (Figure 7a). Next, a PT occurs from the hydronium ion to a nearby water molecule (Figure 7b). A hydrogen bond (HB) is formed between the nascent hydronium ion oxygen and the anion, SO_3^-, while the hydronium has only one water oxygen in its first solvation shell (Figure 7c). Finally, a PT occurs between the hydronium ion and the anion (i.e, $SO_3^- + H_3O^+$), resulting in $SO_3H + H_2O$ (Figure 7d). This procedure will cycle back to the initial condition and restart, as the next PT will occur once SO_3H donates its hydrogen to a nearby water molecule with a first solvation shell consisting of only one water oxygen (Figure 7f), which will result in $SO_3^- + H_3O^+$ (see details in Figure 7e-7h).

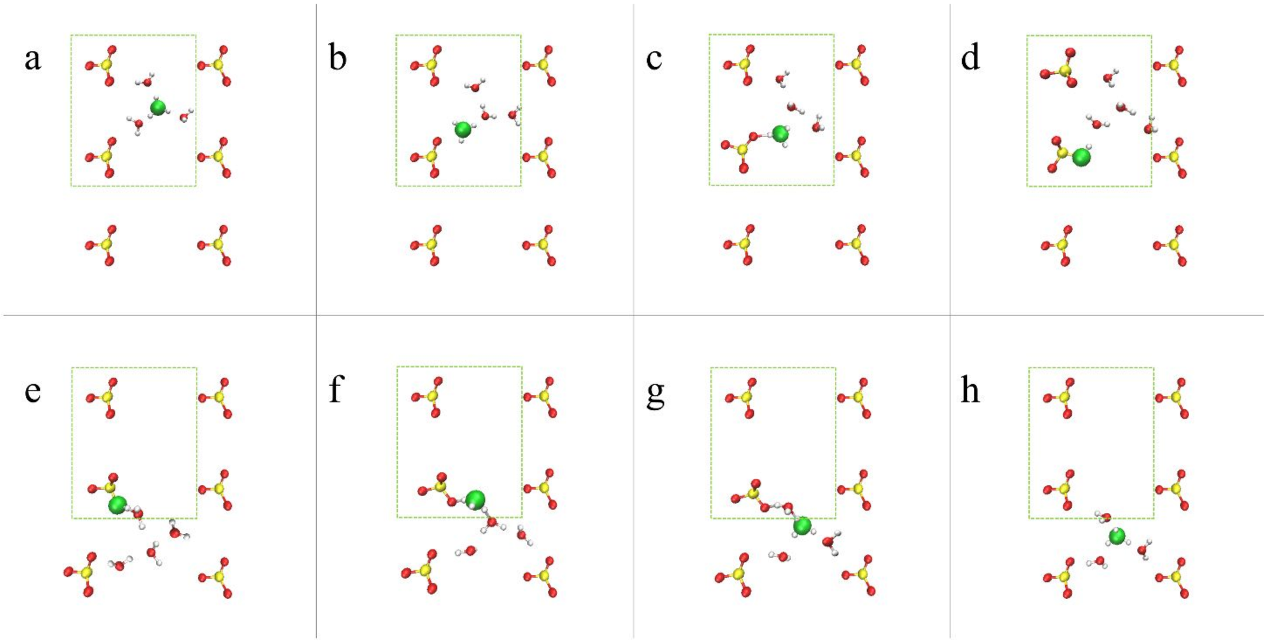

Figure 7: Representative configurations showing the diffusion mechanism for system **λ3** from a *z*-perspective. Red, white, and yellow spheres represent O, H, and S atoms, respectively. A green sphere represents the hydronium ion or SO_3H. The green rectangles show the primitive simulation cell of the system. (a) A hydronium ion in a threefold structure near the anions. (b) A first PT occurs between a water molecule located near an anion and the hydronium ion. (c) A HB is formed between the nascent hydronium ion oxygen and the anion, SO_3^-. (d) The nascent hydronium ion has one water oxygen in its first solvation shell. A PT occurs as a result of the reaction: $SO_3^- + H_3O^+ \leftrightarrow SO_3H + H_2O$. (e) A HB is formed between SO_3H and the nascent water oxygen. (f) The nascent water oxygen (i.e., Onext) has one water oxygen in its first solvation shell. A PT occurs as a result of the reaction: $SO_3H + H_2O \leftrightarrow SO_3^- + H_3O^+$. (g) A PT occurs from H_3O^+ to the nascent water oxygen. (h) The H_3O^+ is back in the center of the simulation cell and is in a threefold solvation structure. The second transfer appears at panels (e) through (h) and happens across the period boundary. For clarity, only water molecules that took part in the diffusion process are presented in the panels.

5. Discussions and Conclusions

The recent work of Trigg, *et al.* 7 reported a combined experimental and theoretical study demonstrating that a hydrated layered membrane can promote proton conductivity on par with current benchmark materials such as Nafion. An innovative and precise polymer design controls polymer folding to achieve a well-ordered layered membrane. X-ray scattering, transmission electron microscopy and all-atom classical molecular dynamics simulates were used to reveal and characterize this and related layered morphologies and electrochemical impedance spectroscopy probed the conductivity of the sulfonated polyethylene, p21SA, membrane. In addition, classical MD simulations were performed to explore the dynamics of water and hydronium ions in this particular material. For this purpose, chain folded molecules of atactic p21SA arranged in layers were studied under hydration values of $3 \leq \lambda \leq 5.5$. The MD simulations suggested that the hydronium ions are close to both the sulfonate groups and to water molecules. Furthermore, the simulations indicated that for a system with $\lambda=3$, hydronium ions are coordinated by zero or one water molecules, while for $\lambda=5.5$, the hydronium coordination environments have either two SO_3^- groups and two waters or one SO_3^- group and three waters (see Figure 3 in Ref. 7).

Comparison of the structural characterization obtained from the classical MD results reported in Ref. 7 with our AIMD graphane bilayer models confirm the picture of the hydronium ion coordination structure in these well-ordered layered membranes. Specifically, both studies show that the hydroniums are located in the vicinity of both the anions and the waters. Secondly, and more importantly, both studies find that the hydronium ions in systems with $\lambda=3$ are more likely to be coordinated by only one water molecule, while for higher hydration values the hydronium ion is more likely to be found with a full threefold coordination shell.

While classical MD simulations enable investigation of relatively large systems and are consider to be a useful tool for structural characterization, their use of empirical force fields with fixed charges mean that they cannot capture chemical bond breaking and forming events, nor do they include manybody polarization, both of which are critical for describing the hydronium structural diffusion process.[95] This limitation motivated our use of AIMD, which allow us to elucidate the atomistic/mechanistic details of the structural diffusion process that drives hydronium ion transport in PEM materials.

Specifically, the AIMD simulation results present here suggest, perhaps somewhat counterintuitively, that the low coordination state of the hydronium ions in system **$\boldsymbol{\lambda}$3** is actually critical for achieving high hydronium conductivity, as the low water content ultimately promotes the reaction: $SO_3^- + H_3O^+ \leftrightarrow SO_3H + H_2O$, which is properly captured in the AIMD simulations and which we find to be an essential part in the hydronium diffusion mechanism. We believe that the discovery of such ion diffusion mechanisms has broad implications on future characterization of new stable polymer electrolyte materials with high ion conductivity.

In order to demonstrate the importance of revealing key principles in the hydronium diffusion mechanism, we find it useful to compare our findings to previously studied hydroxide diffusion mechanisms in analogous AEM environments. While both AEMs and PEMs have been studied extensively over the last decade, it is well known that hydroxide ion conductivity and cation stability remain key hurdles to realizing the full potential of fuel cell based AEMs. In our previous study on hydroxide ion diffusion in model AEMs under low hydration conditions ($2 < \lambda < 5$) [67,68], we found that the water distribution is non-uniform. Comparing to the present study, we find that while the non-uniform water distribution is a common feature of both AEMs and PEMs at low hydration, but the influence of the non-uniform distribution on the hydroxide and hydronium diffusion mechanisms is different. For AEMs, we found that hydroxide ion diffusion is mostly vehicular. This type of diffusion occurs when the water distribution is non-uniform but gives rise to both first and second solvation shells for the hydroxide ions.[68] However, in this study, we find that for PEMs, hydronium ion diffusion is structural rather than vehicular, with the participation of the anions, according to this reaction: $SO_3^- + H_3O^+ \leftrightarrow SO_3H + H_2O$ (as discussed in detail in the previous section). Furthermore, we find that the differences between AEMs and PEMs lie in the essence of the membrane materials. The region between each pair of cations in AEMs was found to create a bottleneck for hydroxide diffusion such that only specific solvation complexes are mobile, leading to a suppression of hydroxide ion diffusion.[68,70] In contrast to AEMs, the model studied here indicates that the anions in PEMs, rather than creating such a bottleneck for hydronium diffusion, they become active participants in the hydronium diffusion mechanism via the reaction $SO_3^- + H_3O^+ \leftrightarrow SO_3H + H_2O$ previously mentioned (see Figure 7), suggesting that under the right hydration conditions, the presence of the anions in the PEM model would promote, rather than suppress, hydronium diffusion. We believe that elucidating the differences between the diffusion mechanisms of the hydroxide and hydronium ions in AEMs and PEMs is the first step towards the discovery and determination of key design principles of new, stable cation or anion conductive membrane materials with high ion conductivity for use in emerging fuel cell technologies and other electrochemical device applications.

In conclusion, in this study, we aimed to uncover atomistic details of the hydronium ion diffusion mechanism in PEMs under confined environments with a layered morphology [7] in order to elucidate the influence of the hydration value on the hydronium ion transport process and to compare our findings to previously studied hydroxide diffusion mechanisms in analogous AEM environments. For this purpose, we simulated two different idealized PEM environments under two hydration conditions ($\lambda = 3$ and 4). We found that the water distribution is uniform for system $\boldsymbol{\lambda}$**4**. However, reducing the number of water molecules per cation by one (system $\boldsymbol{\lambda}$**3**) results in a water distribution that is non-uniform, which is associated with a dearth of water molecules and results in void areas within the simulation cell. We find that the non-uniform water distribution results in an incomplete second solvation shell for the hydronium ion, fewer water molecules in the vicinity of a sulfonate oxygens (i.e., SO_3^-), and a higher probability of obtaining a CN value of ~1 for the oxygen located next to SO_3^-. The existence of these conditions increases the probability that the hydronium ion will react with the anion according to this reaction: $SO_3^- + H_3O^+ \leftrightarrow SO_3H + H_2O$, which was found to be an essential part of the hydronium ion diffusion mechanism at system $\boldsymbol{\lambda}$**3**. Furthermore, we find that under optimal hydration conditions ($\boldsymbol{\lambda}$**3**) the anions in the model PEMs promote hydronium conductivity by playing an active role in the hydronium diffusion mechanism. The results presented in this study enable us to suggest idealized hydration conditions and diffusion mechanisms for achieving high hydronium ion conductivity in high-performance PEM fuel cell devices. We believe this work is the first to provide atomistic insight and a preliminary fundamental understanding of the unique hydronium ion diffusion mechanism in idealized PEMs by using AIMD simulations.

Supplementary Information

The following additional data is presented in the Supplementary Information (SI) for the two systems: (i) system parameters, (ii) OO, O_sO_w and O^*O_w RDFs, (iii) hydronium ion oxygen coordinates as a function of time, (iv) the mean square displacement for water molecules and hydronium ions, and (v) HB criteria for population probabilities of different O* solvation complexes and (vi) further explanation for Figure 5.

Acknowledgments

This work was supported by the National Science Foundation, grant #CHE-1534374 and by the Binational Science Foundation, grant #2018171. Computational resources were provided by the Computational Center for Nanotechnology Innovation at Rensselaer Polytechnic Institute in Troy, New York. KIW acknowledges NSF-DMR-576553.

References

[1] V. Mehta, J.S. Cooper, Review and Analysis of PEM Fuel Cell Design and Manufacturing, J. Power Sources. 114 (2003) 32–53.

[2] A. Kraytsberg, Y. Ein-Eli, Review of Advanced Materials for Proton Exchange Membrane Fuel Cells, Energy Fuels. 28 (2014) 7303−7330.

[3] J. Savage, G.A. Voth, Proton Solvation and Transport in Realistic Proton Exchange Membrane Morphologies, J. Phys. Chem. C. 120 (2016) 3176−3186.

[4] N. Zhang, Y. Song, X. Ruan, X. Yan, Z. Liu, Z. Shen, X. Wuc, G. He, Structural Characteristics of Hydrated Protons in the Conductive Channels: Effects of Confinement and fluorination Studied by Molecular Dynamics Simulation, Phys.Chem.Chem.Phys. 18 (2016) 24198–24209.

[5] F. Sepehr, S.J. Paddison, Primary Hydration and Proton Transfer of Electrolyte Acids: An ab Initio Study, Solid State Ionics. 306 (2017) 2–12.

[6] D.W. Shin, M.D. Guiver, Y.M. Lee, Hydrocarbon-Based Polymer Electrolyte Membranes: Importance of Morphology on Ion Transport and Membrane Stability, Chem. Rev. 117 (2017) 4759−4805.

[7] E.B. Trigg, T.W. Gaines, M. Maréchal, D.E. Moed, P. Rannou, K.B. Wagener, M.J. Stevens, K.I. Winey, Self-Assembled Highly Ordered Acid Layers in Precisely Sulfonated Polyethylene Produce Efficient Proton Transport, Nat. Mater. 17 (2018) 725–731.

[8] A. Albarbar, M. Alrweq, Proton Exchange Membrane Fuel Cell, Springer, Cham, 2018.

[9] M.M. Whistona, I.L. Azevedoa, S. Litsterb, K.S. Whitefoota, C. Samarasc, J.F. Whitacre,

Expert Assessments of the Cost and Expected Future Performance of Proton Exchange Membrane Fuel Cells for Vehicles, PNAS. 116 (2019) 4899–4904.

[10] X. Linga, M. Bonna, K.F. Domkea, S.H. Parekha, Correlated Interfacial Water Transport and Proton Conductivity in Perfluorosulfonic acid Membranes, PNAS. 116 (2019) 8715–8720.

[11] S.A. Roget, P.L. Kramer, J.E. Thomaz, M.D. Fayer, Bulk-like and Interfacial Water Dynamics in Nafion Fuel Cell Membranes Investigated with Ultrafast Nonlinear IR Spectroscopy, J. Phys. Chem. B. 123 (2019) 9408−9417.

[12] Y. Wang, D.F.R. Diaz, K.S. Chen, Z. Wang, X.C. Adroher, Materials, Technological Status, and Fundamentals of PEM Fuel Cells–A Review, Mater. Today. 32 (2020) 178–203.

[13] B.F. Habenicht, S.J. Paddison, M.E. Tuckerman, Ab Initio Molecular Dynamics Simulations Investigating Proton Transfer in Perfluorosulfonic Acid Functionalized Carbon Nanotubes, Phys. Chem. Chem. Phys. 12 (2010) 8728–8732.

[14] B.F. Habenicht, S.J. Paddison, M.E. Tuckerman, The Effects of the Hydrophobic Environment on Proton Mobility in Perfluorosulfonic Acid Systems: An Ab Initio Molecular Dynamics Study, J. Mater. Chem. 20 (2010) 6342–6351.

[15] M.A. Modestino, D.K. Paul, S. Dishari, S.A. Petrina, F.I. Allen, M.A. Hickner, K. Karan, R.A. Segalman, A.Z. Weber, Self-Assembly and Transport Limitations in Confined Nafion Films, Macromolecules. 46 (2013) 867−873.

[16] Z. Yudan, Z. Jian, L. Xiaohua, G. Xiaojing, L. Linghong, Molecular Simulations on Nanoconfined Water Molecule Behaviors for Nanoporous Material Applications, Microfluid Nanofluid. 15 (2013) 191–205.

[17] A. Kusoglu, D. Kushner, D.K. Paul, K. Karan, M.A. Hickner, A.Z. Weber, Impact of Substrate and Processing on Confinement of Nafion Thin Films, Adv. Funct. Mater. 24 (2014) 4763–4774.

[18] K.A. Page, A. Kusoglu, C.M. Stafford, S. Kim, R.J. Kline, A.Z. Weber, Confinement-Driven Increase in Ionomer Thin-Film Modulus, Nano Lett. 14 (2014) 2299−2304.

[19] J.K. Clark II, B.F. Habenichtb, S.J. Paddison, Ab Initio Molecular Dynamics Simulations of Aqueous Triflic Acid Confined in Carbon Nanotubes, Phys. Chem. Chem. Phys. 16 (2014) 16465–16479.

[20] A. Kusoglu, A.Z. Weber, New Insights into Perfluorinated Sulfonic-Acid Ionomers, Chem. Rev. 117 (2017) 987−1104.

[21] A.R. Crothers, C.J. Radke, A.Z. Weber, Impact of Nano- and Mesoscales on Macroscopic Cation Conductivity in Perfluorinated-Sulfonic-Acid Membranes, J. Phys. Chem. C. 121 (2017) 28262−28274.

[22] S.J. Paddison, J.A. Elliott, Molecular Modeling of the Short-Side-Chain Perfluorosulfonic Acid Membrane, J. Phys. Chem. A. 109 (2005) 7583–7593.

[23] S.J. Paddison, K.-D. Kreuer, J. Maier, About the Choice of the Protogenic Group in Polymer Electrolyte Membranes: Ab Initio Modelling of Sulfonic Acid, Phosphonic Acid, and Imidazole Functionalized Alkanes, Phys. Chem. Chem. Phys. 8 (2006) 4530–4542.

[24] R.L. Hayes, S.J. Paddison, M.E. Tuckerman, Proton Transport in Triflic Acid Hydrates Studied via Path Integral Car-Parrinello Molecular Dynamics, J. Phys. Chem. B. 113 (2009) 16574–16589.

[25] R.L. Hayes, S.J. Paddison, M.E. Tuckerman, Proton Transport in Triflic Acid Pentahydrate Studied via Ab Initio Path Integral Molecular Dynamics, J. Phys. Chem. A. 115 (2011) 6112–6124.

[26] J.K. Clark, S.J. Paddison, M. Eikerling, M. Dupuis, J. Thomas A. Zawodzinski, A Comparative Ab Initio Study of the Primary Hydration and Proton Dissociation of Various Imide and Sulfonic Acid Ionomers, J. Phys. Chem. A. 116 (2012) 1801−1813.

[27] C. Wang, S.J. Paddison, Hydration and Proton Transfer in Highly Sulfonated Poly(phenylene sulfone) Ionomers: An Ab Initio Study, J. Phys. Chem. A. 117 (2013) 650–660.

[28] R. Devanathan, N. Idupulapati, M.D. Baer, C.J. Mundy, M. Dupuis, Ab Initio Molecular Dynamics Simulation of Proton Hopping in a Model Polymer Membrane, J. Phys. Chem. B. 117 (2013) 16522−16529.

[29] W. Ensing, J. Hunger, N. Ottosson, H.J. Bakker, On the Orientational Mobility of Water Molecules in Proton and Sodium Terminated Nafion Membranes, J. Phys. Chem. C. 117 (2013) 12930−12935.

[30] J. Savage, Y.-L.S. Tse, G.A. Voth, Proton Transport Mechanism of Perfluorosulfonic Acid Membranes, J. Phys. Chem. C. 118 (2014) 17436−17445.

[31] F. Sepeh, S.J. Paddison, Primary Hydration and Proton Transfer of Electrolyte Acids: An ab Initio Study, Solid State Ion. 306 (2017) 2–12.

[32] B. MacMillan, A. Sharp, R. Armstrong, An NMR Investigation of the Dynamical Characteristics of Water Absorbed in Nafion, Polymer. 40 (1999) 2471−2480.

[33] J.-C. Perrin, S. Lyonnard, A. Guillermo, P. Levitz, Water Dynamics in Ionomer Membranes by Field-Cycling NMR Relaxometry, J. Phys. Chem. B. 110 (2006) 5439−5444.

[34] R. Hammer, M. Schönhoff, M.R. Hansen, Comprehensive Picture of Water Dynamics in Nafion Membranes at Different Levels of Hydration, J. Phys. Chem. B. 123 (2019) 8313−8324.

[35] Y.P. Patil, T.A.P. Seery, M.T. Shaw, R.S. Parnas, In Situ Water Sensing in a Nafion Membrane by Fluorescence Spectroscopy, Ind. Eng. Chem. Res. 44 (2005) 6141–6147.

[36] M.A. Barique, E. Tsuchida, A. Ohira, K. Tashiro, Effect of Elevated Temperatures on the States of Water and Their Correlation with the Proton Conductivity of Nafion, ACS Omega. 3 (2018) 349−360.

[37] H. Nishiyama, S. Takamuku, K. Oshikawa, S. Lacher, A. Iiyama, I. Junji, Chemical States of Water Molecules Distributed Inside a Proton Exchange Membrane of a Running Fuel Cell Studied by Operando Coherent Anti-Stokes Raman Scattering Spectroscopy, J. Phys. Chem. C. 124 (2020) 9703−9711.

[38] K. Schmidt-Rohr, Q. Chen, Parallel Cylindrical Water Nanochannels in Nafion Fuel-Cell Membranes., Nat. Mater. 7 (2008) 75−83.

[39] T. Sasabe, P. Deevanhxay, S. Tsushima, S. Hirai, Investigation on the Effect of

Microstructure of Proton Exchange Membrane Fuel Cell Porous Layers on Liquid Water Behavior by Soft X-Ray Radiography., J. Power Sources. 196 (2011) 8197−8206.

[40] J.A. Elliott, D. Wu, S.J. Paddison, R.B. Moore, A Unified Morphological Description of Nafion Membranes from SAXS and Mesoscale Simulations, Soft Matter. 7 (2011) 6820–6827.

[41] K.D. Kreuer, G. Portale, A Critical Revision of the Nano-Morphology of Proton Conducting Ionomers and Polyelectrolytes for Fuel Cell Applications, Adv. Func. Mater. 23 (2013) 5390—5397.

[42] E.G. Sorte, B.A. Paren, C. G, Rodriguez, C. Fujimoto, C. Poirier, L.J. Abbott, N.A. Lynd, K.I. Winey, A.L.A. Frischknecht, T. M, Impact of Hydration and Sulfonation on the Morphology and Ionic Conductivity of Sulfonated Poly(phenylene) Proton Exchange Membranes, Macromolecules. 52 (2019) 857−876.

[43] L. Yan, C. Rank, S. Mecking, K.I. Winey, Gyroid and Other Ordered Morphologies in Single-Ion Conducting Polymers and Their Impact on Ion Conductivity, J. Am. Chem. Soc. 142 (2020) 857−866.

[44] A. Kusoglu, K. Vezzù, G.A. Hegde, G. Nawn, A.R. Motz, H.N. Sarode, G.M. Haugen, Y. Yang, S. Seifert, M.A.S.H. Yandrasits, C.M. Maupin, A.Z. Weber, V. Di Noto, H.A. M, Transport and Morphology of a Proton Exchange Membrane Based on a Doubly Functionalized Perfluorosulfonic Imide Side Chain Perflourinated Polymer, Chem. Mater. 32 (2020) 38−59.

[45] D. Wu, S.J. Paddison, J.A. Elliottb, A Comparative Study of the Hydrated Mrphologies of Perfluorosulfonic Acid Fuel Cell Membranes with Mesoscopic Simulations, Energy Environ. Sci. 1 (2008) 284–293.

[46] D. Wu, S.J. Paddison, J.A. Elliott, S.J. Hamrock, Mesoscale Modeling of Hydrated Morphologies of 3M Perfluorosulfonic Acid-Based Fuel Cell Electrolytes, Langmuir. 26 (2010) 14308–14315.

[47] E. Negro, M. Vittadello, K. Vezzùd, S.J. Paddison, V. Di Notoa, The Influence of the Cationic Form and Degree of Hydration on the Structure of Nafion, Solid State Ionics. 252

(2013) 84–92.

[48] C. Wang, S.J. Paddison, Mesoscale Modeling of Hydrated Morphologies of Sulfonated Polysulfone Ionomers, Soft Matter. 10 (2014) 819–830.

[49] S. Cui, J. Liu, M.E. Selvan, D.J. Keffer, B.J. Edwards, W. V. Steele, A Molecular Dynamics Study of a Nafion Polyelectrolyte Membrane and the Aqueous Phase Structure for Proton Transport, J. Phys. Chem. B. 111 (2007) 2208–2218.

[50] S. Cui, J. Liu, M.E.S.J.P. Selvan, D.J. Keffer, B.J. Edwards, Comparison of the Hydration and Diffusion of Protons in Perfluorosulfonic Acid Membranes with Molecular Dynamics Simulations, J. Phys. Chem. B. 112 (2008) 13273–13284.

[51] J. XiaO, D. Yan, J. Li, Q. Li, H. Sun, Hydronium Ions Diffusion Behavior in Nafion Membrane By Mesoscopic Simulation, AIP Adv. 8 (2018) 0753030–075314.

[52] J.A. Elliotta, S.J. Paddison, Modelling of Morphology and Proton Transport in PFSA Membranes, Phys. Chem. Chem. Phys. 9 (2007) 2602–2618.

[53] J. Savage, G.A. Voth, Persistent Subdiffusive Proton Transport in Perfluorosulfonic Acid Membranes, J. Phys. Chem. Lett. 5 (2014) 3037−3042.

[54] S. Liu, J. Savage, G.A. Voth, Mesoscale Study of Proton Transport in Proton Exchange Membranes: Role of Morphology, J. Phys. Chem. C. 119 (2015) 1753−1762.

[55] S. Sengupta, A. V. Lyulin, Molecular Modeling of Structure and Dynamics of Nafion Protonation States, J. Phys. Chem. B. 123 (2019) 6882−6891.

[56] E. Spohr, Molecular Dynamics Simulations of Proton Transfer in a Model Nafion Pore, Mol. Simul. 30 (2004) 107–115.

[57] Y.-L.S. Tse, A.M. Herring, K. Kim, G.A. Voth, Molecular Dynamics Simulations of Proton Transport in 3M and Nafion Perfluorosulfonic Acid Membranes, J. Phys. Chem. C. 117 (2013) 8079−8091.

[58] C. Arntsen, J. Savage, Y.-L.S.Tse, G.A.Voth, Simulation of Proton Transport in Proton Exchange Membranes with Reactive Molecular Dynamics, Fuel Cells. 6 (2016) 695–703.

[59] C. Zheng, F. Geng, Z. Rao, Proton Mobility and Thermal Conductivities of Fuel Cell

Polymer Membranes: Molecular Dynamics Simulation, Comput. Mater. Sci. 132 (2017) 55–61.

[60] S.J. Paddison, The Modeling of Molecular Structure and Ion Transport in Sulfonic Acid Based Ionomer Membranes, J. New Mater. Electrochem. Syst. 4 (2001) 197−207.

[61] A. Roudgar, S.P. Narasimachary, M. Eikerling, Ab Initio Study of Surface-Mediated Proton Transfer in Polymer Electrolyte Membranes, Chem. Phys. Lett. 457 (2008) 337–341.

[62] Y.-K. Choe, E. Tsuchida, T. Ikeshoji, S. Yamakawa, Nature of Proton Dynamics in A Polymer Electrolyte Membrane, Nafion: A First-Principles Molecular Dynamics Study, Phys. Chem. Chem. Phys. 11 (2009) 3892–3899.

[63] B.F. Habenicht, S.J. Paddison, M.E. Tuckerman, The Effects of the Hydrophobic Environment on Proton Mobility in Perfluorosulfonic Acid Systems: An Ab Initio Molecular Dynamics Study, J. Mater. Chem. 20 (2010) 6342–6351.

[64] M.A. Ilhan, E. Spohr, Hydrogen Bonding in Narrow Protonated Polymer Electrolyte Pores, J. Electroanal. Chem. 660 (2011) 347–351.

[65] T.C. Berkelbach, H.-S. Lee, M.E. Tuckerman, Concerted Hydrogen-Bond Dynamics in the Transport Mechanism of the Hydrated Proton: A First-Principles Molecular Dynamics Study, Phys.Rev.Lett. 103 (2009) 238302–238305.

[66] Y.-L.S. Tse, C. Knight, G.A. Voth, An Analysis of Hydrated Proton Diffusion in Ab Initio Molecular Dynamics, J. Chem. Phys. 142 (2015) 014104–014117.

[67] T. Zelovich, Z. Long, M. Hickner, S.J. Paddison, C. Bae, M.E. Tuckerman, Ab initio Molecular Dynamics Study of Hydroxide Diffusion Mechanisms in Nano-Confined Structural mimics of Anion Exchange Membranes, J. Phys. Chem. C. 123 (2019) 4638–4653.

[68] T. Zelovich, L. Vogt-Maranto, M. Hickner, S.J. Paddison, C. Bae, D.R. Dekel, M.E. Tuckerman, Hydroxide Ion Diffusion in Anion Exchange Membranes at Low Hydration: Insights from Ab initio Molecular Dynamics, Chem. Mater. 31 (2019) 5778–5787.

[69] T. Zelovich, M.E. Tuckerman, Water Layering Affects Hydroxide Diffusion in Functionalized Nanoconfined Environments, J. Phys. Chem. Lett. 11 (2020) 5087–5091.

[70] T. Zelovich, L. Vogt-Maranto, M. Hickner, S.J. Paddison, C. Bae, M.E. Tuckerman, Non-Monotonic Temperature Dependence of Hydroxide Diffusion in Model Anion Exchange Membranes Based on Functionalized Nanoconfined Environments, J. Membr. Sci. (in Revis. (2020).

[71] M.E. Tuckerman, K. Laasonen, M. Sprik, M. Parrinello, Ab Initio Molecular Dynamics Simulation of the Solvation and Transport of Hydronium and Hydroxyl Ions in Water, J. Chem. Phys. 103 (1995) 150–161.

[72] M. Tuckerman, K. Laasonen, M. Sprik, M. Parrinello, Ab Initio Molecular Dynamics Simulation of the Solvation and Transport of H_3O^+ and OH^- Ions in Water, J. Phys. Chem. 99 (1995) 5749–5752.

[73] D. Marx, M.E. Tuckerman, J. Hutter, M. Parrinello, The Nature of the Hydrated Excess Proton in Water, Nature. 397 (1999) 601–604.

[74] M.E. Tuckerman, D. Marx, M. Parrinello, The Nature and Transport Mechanism of Hydrated Hydroxide Ions in Aqueous Solution, Nature. 417 (2002) 925–929.

[75] M.E. Tuckerman, A. Chandra, D. Marx, Structure and Dynamics of OH - (aq), Acc. Chem. Res. 39 (2006) 151–158.

[76] A. Chandra, M.E. Tuckerman, D. Marx, Connecting Solvation Shell Structure to Proton Transport Kinetics in Hydrogen – Bonded Networks via Population Correlation Functions, Phys. Rev. Lett. 99 (2007) 145901–145904.

[77] D. Marx, A. Chandra, M.E. Tuckerman, Aqueous Basic Solutions : Hydroxide Solvation , Structural Diffusion , and Comparison to the Hydrated Proton, Chem. Rev. 110 (2010) 2174–2216.

[78] M.E. Tuckerman, A. Chandra, D. Marx, A Statistical Mechanical Theory of Proton Transport Kinetics in Hydrogen-Bonded Networks Based On Population Correlation Functions With Applications to Acids and Bases, J. Chem. Phys. 133 (2010) 124108–124129.

[79] Z. Ma, M.E. Tuckerman, On the Connection Between Proton Transport , Structural Diffusion , and Reorientation of the Hydrated Hydroxide Ion as a Function of Temperature, Chem. Phys. Lett. 511 (2011) 177–182.

[80] A. Hassanali, F. Giberti, J. Cuny, T.D. Kühne, M. Parrinello, Proton transfer through the water gossamer, PNAS. 110 (2013) 13723–13728.

[81] N. Agmon, H.J. Bakker, R.K. Campen, R.H. Henchman, P. Pohl, S. Roke, M. Thamer, A. Hassanali, Protons and Hydroxide Ions in Aqueous Systems, Chem. Rev. 116 (2016) 7642−7672.

[82] F. Sepehr, H. Liu, X. Luo, C. Bae, M.E. Tuckerman, M.A. Hickner, S.J. Paddison, Mesoscale Simulations of Anion Exchange Membranes Based on Quaternary Ammonium Tethered Triblock Copolymers, Macromolecules. 50 (2017) 4397–4405.

[83] M.E. Tuckerman, Ab Initio Molecular Dynamics: Basic Concepts, Current Trends and Novel Applications, J. Phys. Condens. Matter. 14 (2002) R1297–R1355.

[84] D. Marx and J. Hutter, Ab Initio Molecular Dynamics: Theory and Implementation, in Modern Methods and Algorithms of Quantum Chemistry, Vol.1, Forschungszentrum, Juelich, 2000.

[85] D.M. J. Hutter, A. Alavi, T. Deutsch, M. Bernasconi, S. Goedecker, M.T. and M. Parrinello, CPMD, IBM Corporation 1990–2009 and MPI für Festkörperforschung 1997–2001; see www.cpmd.org, 2009, (n.d.).

[86] G.J. Martyna, M.E. Tuckerman, M.L. Klein, Nose-Hoover Chains: The Canonical Ensemble via Continuous Dynamics, J. Chem. Phys. 97 (1992) 2635–2643.

[87] P.C. Aeberhard, J.S. Arey, I.-C. Lin, U. Rothlisberger, Accurate DFT Descriptions for Weak Interactions of Molecules Containing Sulfur, JCTC. 5 (2009) 23–28.

[88] I.-C. Lin, M.D. Coutinho-Neto, C. Felsenheimer, O.A. von Lilienfeld, I. Tavernelli, U. Rothlisberger, Library of Dispersion-Corrected Atom-Centered Potentials for Generalized Gradient Approximation Functionals: Elements H, C, N, O, He, Ne, Ar, and Kr, Phys. Rev. B. 75 (2007) 205131–205135.

[89] A. D. Becke, Density-Functional Exchange-Energy Approximation With Correct Asymptotic Behavior, Phys. Rev. A. 38 (1988) 3098–3100.

[90] C. Lee, W. Yang, R.G. Parr, Development of the Colle-Salvetti Correlation-Energy Formula into A Functional of the Electron Density, Phys. Rev. B. 37 (1988) 785–789.

[91] G.R. Jenness, O. Karalti, K.D. Jordan, Benchmark Calculations of Water–Acene Interaction Energies: Extrapolation to The Water–Graphene Limit and Assessment of Dispersion–Corrected DFT Methods, Phys. Chem. Chem. Phys. 12 (2010) 6375–6381.

[92] I.-C. Lin, A.P. Seitsonen, I. Tavernelli, U. Rothlisberger, Structure and Dynamics of Liquid Water from ab Initio Molecular Dynamics - Comparison of BLYP, PBE, and revPBE Density Functionals with and without van der Waals Corrections, J. Chem. Theory Comput. 8 (2012) 3902−3910.

[93] Z. Zhu, M.E. Tuckerman, Ab Initio Molecular Dynamics Investigation of the Concentration Dependence of Charged Defect Transport in Basic Solutions via Calculation of the Infrared Spectrum, J. Phys. Chem. B. 106 (2002) 8009–8018.

[94] J.A. Morrone, K.E. Haslinger, M.E. Tuckerman, Ab Initio Molecular Dynamics Simulation of the Structure and Proton Transport Dynamics of Methanol-Water Solutions, J. Phys. Chem. B. 110 (2006) 3712–3720.

[95] G. Brancato, M.E. Tuckerman, A Polarizable Multistate Empirical Valence Bond Model for Proton Transport in Aqueous Solution, J. Chem. Phys. 122 (2005) 224507–224517.